Yasuda *Earth, Planets and Space* 2014, **66**:34
http://www.earth-planets-space.com/content/66/1/34

Earth, Planets and Space
a SpringerOpen Journal

FULL PAPER Open Access

A new technique using FT-IR micro-reflectance spectroscopy for measurement of water concentrations in melt inclusions

Atsushi Yasuda

Abstract

This paper presents a new technique to measure water concentrations in small volcanic glasses such as melt inclusions. The technique uses Fourier transform infrared (FT-IR) micro-reflectance spectroscopy, and thus does not require a doubly polished sample. To enhance the signal-to-noise (S/N) ratio, a vacuum pump and a narrow-band mercury-cadmium-telluride (MCT) detector were introduced into the FT-IR spectrometer. The pump reduced noise caused by atmospheric water vapor and carbon dioxide, and the detector enhanced the signal, which resulted in significant improvement of the S/N ratio. For standards, we synthesized 32 glasses with different water concentrations ranging from basaltic to rhyolitic composition. An empirical relationship was established between total water content and the negative peak height normalized by the baseline extrapolated from the neighboring region ($\Delta R/R_{\mathrm{baseline}}$); for example, H_2O wt.% = $49.76 \times \Delta R/R_{\mathrm{baseline}} - 0.08$ for basaltic composition. The regression error corresponded to approximately 0.29 wt.% water (2σ) with an aperture of 20 μm × 20 μm and 2,048 scans. To apply the technique to natural samples of various shapes, we developed a method to correct the spectrum of melt inclusion contaminated with host minerals. This method calculates the overlapping volume of the host crystal using the reflectance spectra at 800 to 1,300 cm^{-1} and is applicable to melt inclusions hosted by olivine, orthopyroxene, and plagioclase.

Keywords: Water; FT-IR; Reflectance spectroscopy; Melt inclusion

Background

Water in magma strongly affects how a volcano erupts (e.g., Roggensack et al. 1997; Métrich et al. 2001). Therefore, it is important to determine the amount of water dissolved in magma to predict how an eruption develops (Bureau et al. 1998; Luhr 2001; Saito et al. 2001; Wallace 2005; Métrich and Wallace 2008). Fourier transform infrared (FT-IR) transmission analysis is considered to be an effective method to determine the volatile content in magmas (e.g., Stolper 1982; Dixon et al. 1995). It was successfully applied to small volcanic glasses such as melt inclusions to estimate pre-eruptive water content in magma (e.g., Luhr 2001; Saito et al. 2001). However, sample preparation for this method is difficult. Specifically, this method requires fragile samples with thicknesses of several tens of micrometers to be parallel and flatly polished on both sides. Therefore, its practical usage is not easy.

Previously, FT-IR micro-reflectance spectroscopy was proposed as an efficient method to determine water concentrations in volcanic glasses because of its great advantage in regards to sample preparation, i.e., it requires neither doubly polished wafers nor knowledge of the sample thickness (Grzechnik et al. 1996; Moore et al. 2000; Hervig et al. 2003, King and Larsen 2013). Hervig et al. (2003) reported that the height of the peaks in the reflectance spectra of synthesized hydrous glasses appeared to correlate positively with the water concentration of the sample. However, to date, application of this method to natural samples has been very limited (Larsen 2008); this is because the intensity of the reflectance signal related to water absorption is generally much weaker than that observed in a transmittance spectrum. Thus, reflectance spectra are too noisy to make precise quantitative measurements especially when analyzing small samples such as melt inclusions. Recently, Lowenstern

Correspondence: yasuda@eri.u-tokyo.ac.jp
Earthquake Research Institute, University of Tokyo, Yayoi 1-1-1, Bunkyo-ku, Tokyo 113-0032, Japan

and Pitcher (2013) overcame this difficulty by using attenuated total reflectance (ATR) FT-IR spectroscopy. Multiple internal reflections between the ATR crystal and the sample enhance the signal of water absorption. However, the technique can damage very fragile samples because the sample is pressed into direct contact with the hard ATR crystal.

The key for solving this problem is to reduce noise and improve the signal-to-noise (S/N) ratio. Recently, Yasuda (2011) used a vacuum FT-IR apparatus to reduce noise of reflectance spectra and measured water content of olivine-hosted melt inclusions with diameters as small as 30 μm. With this technique, olivine-hosted melt inclusions from the 2011 eruption of the Mt. Kirishima volcano were analyzed for water content, and the results were successfully used to establish a constraint on the depth of the basaltic andesite magma reservoir (Suzuki et al. 2013). Thereafter, we made several additional improvements in both hardware and software, and recently, it has become possible to measure water content with reasonable accuracy in melt inclusions with diameters as small as 20 μm. The details of this technique are reported herein.

Methods

Analytical instrument

All measurements were performed using a vacuum FT-IR system installed at the Earthquake Research Institute (ERI), University of Tokyo. The system is composed of a JASCO FT/IR-660 Plus spectrometer and a JASCO IRT-30 microscope. The FT-IR system is equipped with a KBr beamsplitter, a globar infrared source, ×32 Cassegrain mirror with a maximum incident angle of 45°, and two mercury-cadmium-telluride (MCT) detectors (mid-band and narrow-band).

The narrow-band MCT detector is much more sensitive than the mid-band MCT detector at the cost of a narrower spectral range. Compared with the mid-band MCT detector, the narrow-band MCT detector offers an S/N ratio that is about five times better at 800 to 5,500 cm^{-1} than the mid-band MCT detector (Figure 1a). Therefore, we used the narrow-band MCT in this study.

The most important feature of the system is the adoption of a rotary vacuum pump to evacuate the entire beam path below several tens of Pascal (Pa). The removal of atmospheric CO_2 and water vapor by evacuation quite effectively reduces their noisy absorption at approximately 3,650, 2,400, and 1,630 cm^{-1}. Although purging with dry N_2 gas is another way to reduce this noise source (Hervig et al. 2003), it requires longer time periods to reduce the noise to the level obtained by the evacuation. Specifically, it requires only 5 min to obtain a stable signal by the evacuation method, but it requires 50 min to obtain a stable signal when purging with dry N_2 gas at 10 l/min.

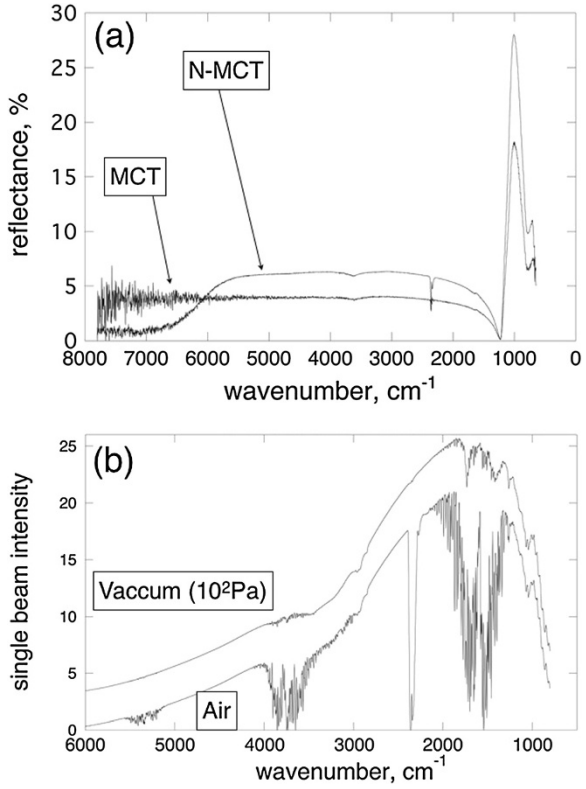

Figure 1 Comparisons of reflectance spectra. (a) Comparison of a reflectance spectrum obtained using a narrow-band detector (N-MCT) with that using a mid-band detector (MCT). Sample contains 3.4 wt.% water. Both spectra were obtained with an aperture of 30 μm × 30 μm and 1,024 scans in air. A gold mirror was used as a reflectance reference. The reflectance signal from the gold mirror was saturated at wavenumbers below 6,000 cm^{-1} when the N-MCT detector was used. Therefore, reflectance of the glass sample was higher than that expected from the refractive index of the glass sample. **(b)** Comparison of a reflectance spectrum obtained at 100 Pa with that obtained in air. Both spectra were obtained with an aperture of 50 μm × 50 μm and 2,048 scans against a gold mirror using an MCT detector.

Moreover, evacuating the entire beam path has the additional advantage that the IR intensity arriving at the detector becomes slightly stronger by virtue of the absence of the fluctuations in the air. Figure 1b shows the effectiveness of the vacuum system to reduce noise. These two hardware modifications improved the S/N ratio remarkably, as shown in Figure 2.

Synthesis of hydrous glass standards

By using a KOBELCO internally heated pressure vessel at ERI and with Ar as the pressurizing medium, we synthesized 32 glasses with various water concentrations ranging from basaltic to rhyolitic composition. The composition of the glasses and the conditions of their synthesis are summarized in Table 1. In each experiment, approximately 250 mg of fine rock powder with a known

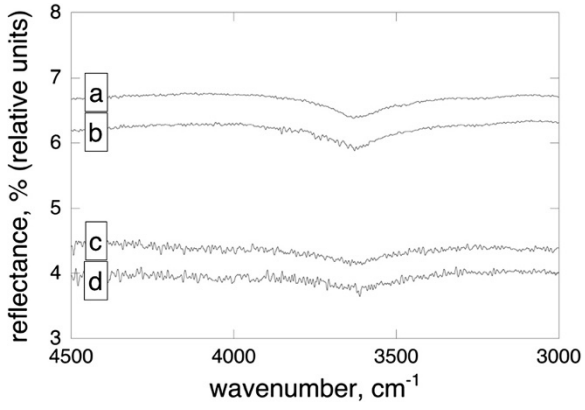

Figure 2 Comparisons of reflectance spectra obtained under different conditions. Reflectance spectra are compared between **(a)** vacuum and N-MCT, **(b)** air and N-MCT, **(c)** vacuum and MCT, and **(d)** air and MCT. All spectra were obtained with an aperture of 30 μm × 30 μm and 1,024 scans on a basaltic glass containing 3.4 wt.% water. The plots are offset for clarity.

composition was loaded into a $\phi = 6.0/5.7$ mm $Au_{75}Pd_{25}$ tube with a certain volume of distilled water, and then both ends of the tube were welded shut. Runs lasted from 7 to 24 h, depending on the water content. Subsequently, the sample was crushed into pieces approximately 1 mm in size, and several pieces were mounted in an epoxy resin to check the compositional homogeneity of the sample. Then, it was analyzed with a JXA-8800R electron probe micro-analyzer at ERI. Minute inspection of backscattered electron images of the glass revealed that the glass was free of both bubbles and crystals. Major element compositions of the glass were determined with an accelerating voltage of 15 kV, a beam current of 12 nA, and a counting time of 15 and 7 s for peak and background, respectively. The beam diameter was set to 10 μm to minimize Na loss. Nine to 11 analyses were performed on each glass chip, and the results assured its chemical homogeneity.

The water content of the glasses was measured using a Karl Fischer titration vessel (Kyoto Denshi, MKC-610) attached to an evaporator for rock powder (Kyoto Denshi, ADP512). Water released from the sample was moved into the titration vessel by carrier gas. The carrier gas consisted of dry N_2 gas with a small amount of O_2 and had a flow rate of 200 ml/min. A sample on a molybdenum boat was placed in a heating tube and preheated in a first furnace at 120°C for several minutes to remove moisture until it reached a stable background signal of <0.2 μg/s water titration rate. Then, the boat was moved to a second furnace at 1,000°C to extract dissolved water from the sample. The titration endpoint was determined when the signal lowered below the background.

Depending on the water content of the standard glasses, 50 to 100 mg of recovered charge was crushed below 20 μm and prepared for the Karl Fischer measurement. A typical measurement time was shorter than 10 min, but some samples with higher water content took as long as 20 min to reach the titration endpoint. The water content was calculated as

$$H_2O\,\mathrm{wt.\%} = 100\,(L–B \times t)/w,$$

where L is the total titration (μg), B is the background (μg/s), t is the measurement time (s), and w is the sample weight (μg).

Since the background could fluctuate during measurements, we estimated the maximum uncertainty in the titration rate caused by background fluctuation to be 0.1 μg/s based on repeated analyses of minerals with known stoichiometry. Taking into account the uncertainty derived from the measurement of the sample weight, this resulted in a maximum uncertainty of ±0.15 wt.% for a typical measurement of the synthetic glass samples.

FT-IR analysis

Before analysis with the FT-IR apparatus, the standard glasses were mounted in an epoxy resin, and then singly polished with a 1-μm grain diamond paste. Prior to loading sample into the microscopic chamber, the IR source and interferometer were evacuated below 100 Pa. After approximately 5 min of evacuation, the pressure of the microscope chamber decreased below 50 Pa, and then FT-IR measurements were started. A gold mirror was used as a standard reference for all FT-IR reflection measurements. The spectral range of a typical measurement was 800 to 5,500 cm^{-1}. Several microscope apertures ranging in size from 20 × 20 to 100 × 100 μm were tested for noise level. Normally, 1,024 or 2,048 scans were collected at a resolution of 4 cm^{-1}. It took 22 min to collect 2,048 scans. Both samples and the reference were set on a holder. Therefore, measurements were performed sequentially from reference to samples without opening the microscope chamber.

The change in reflectance intensity was determined as follows: (1) First, a 25-point moving average was applied to the raw data; (2) the baseline curve was established by fitting the background data to a fourth-degree polynomial. Data within the ranges 2,000 to 2,800 and 4,600 to 5,400 cm^{-1} were used in fitting the polynomial baseline curve to the data. (3) After subtracting the baseline curve from the data, ΔR was defined as the maximum amplitude of the signal at approximately 3,650 cm^{-1}, and R_{baseline} was defined as the reflectance of the baseline curve at the wavenumber where the signal had maximum amplitude. (4) The $\Delta R/R_{\mathrm{baseline}}$ ratio was calculated. Figure 3 summarizes these definitions.

As discussed by Hervig et al. (2003), it is important to normalize the ΔR to a reflectance taken close to, but

Table 1 Run conditions for synthesized standard glasses and their infrared data

Sample ID	Composition[a]	*T* (°C)	*P* (MPa)	Duration (h)	H_2O (wt.%)[b]	$\Delta R/R_{baseline}$	Aperture size (μm)	Scan number
ED1-0	R	1,240	0.1	2	0.17	0.0038	20 × 20	2,048
ED1-1	R	1,220	152	22	4.16	0.0957	20 × 20	2,048
ED1-4	R	1,200	125	22	3.05	0.0719	20 × 20	2,048
ED1-5	R	1,220	168	23	3.49	0.0789	20 × 20	2,048
EJA3-0A	A	1,240	0.1	2	0.15	0.0059	100 × 100	1,024
EJA3-0B	A	1,240	0.1	2	0.15	0.0052	30 × 30	2,048
EJA3-1	A	1,200	108	23	1.12	0.0209	100 × 100	1,024
EJA3-2	A	1,200	109	23	1.82	0.0425	100 × 100	1,024
EJA3-3A	A	1,220	168	23	2.52	0.0409	100 × 100	1,024
EJA3-3B	A	1,220	168	23	2.52	0.0438	30 × 30	2,048
EJA3-4	A	1,220	204	22	3.27	0.0675	100 × 100	1,024
EJA3-5	A	1,150	249	21	4.59	0.1078	100 × 100	1,024
EJA3-6	A	1,150	313	22	5.11	0.1012	100 × 100	1,024
EJA3-7A	A	1,170	331	18	5.04	0.1003	100 × 100	1,024
EJA3-7B	A	1,170	331	18	5.04	0.1097	30 × 30	2,048
EJA3-9	A	1,240	110	8	0.55	0.0113	100 × 100	1,024
EJB2-0A	B1	1,240	0.1	2	0.14	0.0030	20 × 20	2,048
EJB2-0B	B1	1,240	0.1	2	0.14	0.0064	100 × 100	1,024
EJB2-1A	B1	1,240	140	7	2.16	0.0438	20 × 20	2,048
EJB2-1B	B1	1,240	140	7	2.16	0.0418	100 × 100	1,024
EJB2-3A	B1	1,220	164	22	1.78	0.0401	20 × 20	2,048
EJB2-3B	B1	1,220	164	22	1.78	0.0337	100 × 100	1,024
EJB2-4A	B1	1,230	175	19	1.21	0.0237	20 × 20	2,048
EJB2-4B	B1	1,230	175	19	1.21	0.0210	100 × 100	1,024
EJB2-5A	B1	1,200	185	8	4.11	0.0815	20 × 20	2,048
EJB2-5B	B1	1,200	185	8	4.11	0.0765	100 × 100	1,024
EJB2-6A	B1	1,220	308	23	4.29	0.0828	20 × 20	2,048
EJB2-6B	B1	1,220	308	23	4.29	0.0797	100 × 100	1,024
EJB2-7A	B1	1,220	164	24	2.26	0.0468	20 × 20	2,048
EJB2-7B	B1	1,220	164	24	2.26	0.0432	100 × 100	1,024
EJB2-8A	B1	1,240	110	8	0.52	0.0130	20 × 20	2,048
EJB2-8B	B1	1,240	110	8	0.52	0.0159	100 × 100	1,024
EJB2-12A	B1	1,220	204	22	0.51	0.0135	20 × 20	2,048
EJB2-12B	B1	1,220	204	22	0.51	0.0139	100 × 100	1,024
EJB2-13A	B1	1,200	188	17	3.33	0.0708	20 × 20	2,048
EJB2-13B	B1	1,200	188	17	3.33	0.0674	100 × 100	1,024
EJB3-00A	B2	1,240	0.1	2	0.15	0.0044	30 × 30	2,048
EJB3-00B	B2	1,240	0.1	2	0.15	0.0048	100 × 100	1,024
EJB3-1A	B2	1,240	156	21	2.84	0.0600	30 × 30	2,048
EJB3-1B	B2	1,240	156	21	2.84	0.0577	100 × 100	1,024
EJB3-2A	B2	1,220	162	21	1.86	0.0361	30 × 30	2,048
EJB3-2B	B2	1,220	162	21	1.86	0.0342	100 × 100	1,024
EJB3-3A	B2	1,220	162	21	2.65	0.0532	30 × 30	2,048
EJB3-3B	B2	1,220	162	21	2.65	0.0473	100 × 100	1,024

Table 1 Run conditions for synthesized standard glasses and their infrared data *(Continued)*

EJB3-4A	B2	1,230	175	19	1.32	0.0279	30 × 30	2,048
EJB3-4B	B2	1,230	175	19	1.32	0.0249	100 × 100	1,024
EJB3-6A	B2	1,150	249	21	4.34	0.0919	30 × 30	2,048
EJB3-6B	B2	1,150	249	21	4.34	0.0923	100 × 100	1,024
EJB3-7A	B2	1,220	290	21	4.32	0.0863	30 × 30	2,048
EJB3-7B	B2	1,220	290	21	4.32	0.0864	100 × 100	1,024
EJB3-8	B2	1,150	195	17	3.40	0.0763	30 × 30	2,048
EJB3-9A	B2	1,240	110	8	0.62	0.0165	30 × 30	2,048
EJB3-9B	B2	1,240	110	8	0.62	0.0148	100 × 100	1,024

[a]Glass compositions; R (rhyolite): SiO_2 = 73.5, TiO_2 = 0.3, Al_2O_3 = 13.5, FeO = 2.5, MnO = 0.1, MgO = 0.9, CaO = 2.5, Na_2O = 4.2, K_2O = 2.4; A (andesite): SiO_2 = 62.8, TiO_2 = 0.7, Al_2O_3 = 15.7, FeO = 5.9, MnO = 0.1, MgO = 3.8, CaO = 6.3, Na_2O = 3.2, K_2O = 1.4; B1 (basalt): SiO_2 = 53.6, TiO_2 = 1.2, Al_2O_3 = 14.8, FeO = 13.1, MnO = 0.2, MgO = 4.7, CaO = 9.9, Na_2O = 2.1, K_2O = 0.4; B2 (basalt): SiO_2 = 51.3, TiO_2 = 1.5, Al_2O_3 = 17.3, FeO = 10.8, MnO = 0.2, MgO = 5.2, CaO = 9.9, Na_2O = 2.8, K_2O = 0.8.
[b]H_2O (wt.%) determined by Karl Fischer titration.

distinct from, the negative peak caused by water absorbance. In the present study, the ΔR depends on the distance between the sample surface and the focal point of the Cassegrain mirror. Both under-focusing and over-focusing decrease ΔR. It has yet to be clarified whether the observed dependence was a characteristic peculiar to the FT-IR apparatus used in the present study. The $\Delta R/R_{\mathrm{baseline}}$ ratio, however, still remains virtually constant. Therefore, we adopted the $\Delta R/R_{\mathrm{baseline}}$ ratio as a key value.

Results and discussion

Empirical calibration

Analytical results for the synthesized glasses are given in Table 1. Figure 4 shows the change in the intensity of the normalized reflectance signal $\Delta R/R_{\mathrm{baseline}}$ plotted against the concentration of water dissolved in the synthesized glasses. The results show that $\Delta R/R_{\mathrm{baseline}}$ values increased linearly with the water concentration. Linear least squares fitting of the data gave the following regression equations: water (wt.%) = (49.76 ± 1.10 (1σ)) × $\Delta R/R_{\mathrm{baseline}}$ − 0.08 for basaltic composition (Figure 4a),

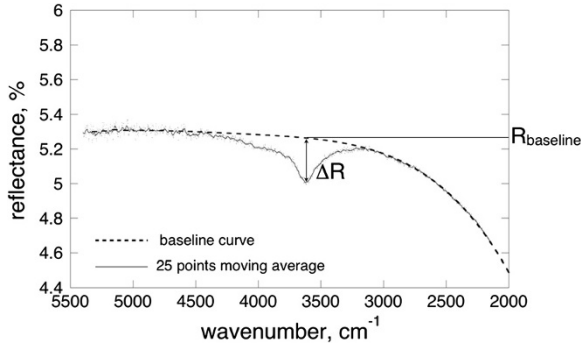

Figure 3 Definition of $\Delta R/R_{\mathrm{baseline}}$. Raw data are plotted as dots. A fourth-degree polynomial was used for the baseline curve (dashed curve).

water (wt.%) = (46.74 ± 2.52) × $\Delta R/R_{\mathrm{baseline}}$ + 0.10 for andesitic composition (Figure 4b), and water (wt.%) = (43.51 ± 1.02) × $\Delta R/R_{\mathrm{baseline}}$ − 0.004 for rhyolitic composition (Figure 4c). The standard error (2σ) of the regression and the standard deviation of the slopes were calculated in accordance with the method of Miller (1991). The standard error (2σ) of the regression was 0.29 wt.% water for basaltic composition. It was slightly larger for the other compositions, however, because of their inferior fitting. Note that the slopes determined here depend on the incident angle of the beam on the sample, which is determined by the Cassegrain mirror. Therefore, the proposed method requires calibration for different optical settings.

Effect of the aperture size on analysis was evaluated by using the basaltic composition (Table 1), and the effect was found to be insignificant. The regression equation for the larger aperture size (100 μm × 100 μm) was expressed as water (wt.%) = (51.92 ± 1.55) × $\Delta R/R_{\mathrm{baseline}}$ − 0.06. Although the slope appears to be a little bit steeper than that obtained with the smaller aperture, the difference was statistically insignificant at the 95% confidence level.

The slope for rhyolitic glass was slightly lower than that for basaltic glass. It is noteworthy, however, that the compositional dependence was much weaker than that of the molar absorptivity for transmission infrared spectroscopy. The transmission molar absorptivity at 3,550 cm^{-1} changes by approximately 50% from basaltic glasses to rhyolitic glasses (Zhang 1999). The low sensitivity of reflectivity to the silicate composition observed in the present study is consistent with previous studies (Hervig et al. 2003; Lowenstern and Pitcher 2013).

The Kramers-Kronig transform procedure provides another method to deduce water content of a sample from its reflectance spectra (Grzechnik et al. 1996; King and Larsen 2013). However, we did not apply this procedure in the present study, partly because the quite linear relationship between $\Delta R/R_{\mathrm{baseline}}$ and water content was sufficient for determining the water content of the

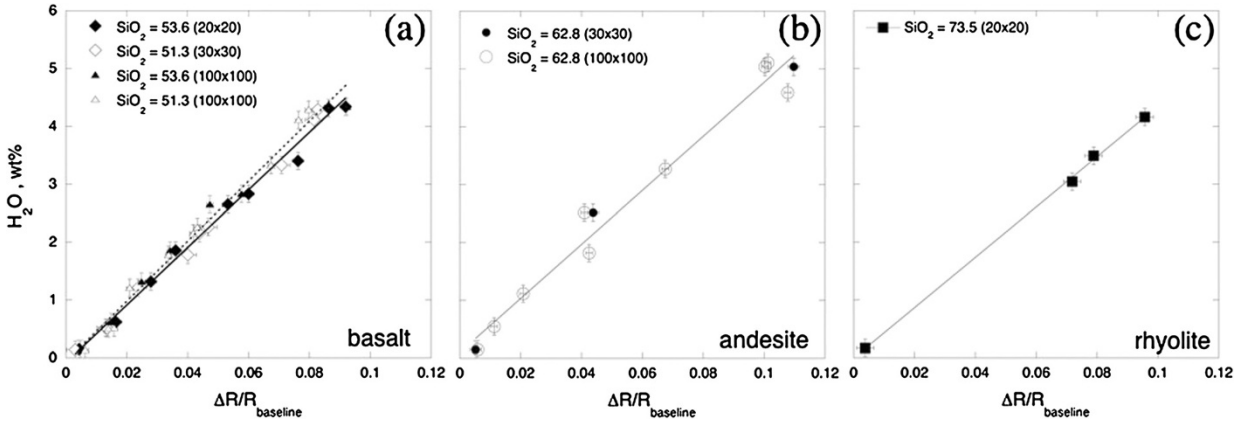

Figure 4 Empirical calibration of the reflectance signal for water concentration. Composition of synthesized glasses and their measurement conditions are listed in Table 1. **(a)** Basaltic composition. Two regression lines correspond to the difference of aperture size; larger (100 × 100 μm) (dotted line): water (wt.%) = (51.92 ± 1.55) × $\Delta R/R_{\text{baseline}}$ − 0.06 (r^2 = 0.990), and smaller (20 × 20 μm and 30 × 30 μm) (solid line): water (wt.%) = (49.76 ± 1.10) × $\Delta R/R_{\text{baseline}}$ − 0.08 (r^2 = 0.992). **(b)** Andesitic composition: water (wt.%) = (46.74 ± 2.52) × $\Delta R/R_{\text{baseline}}$ + 0.10 (r^2 = 0.975). **(c)** Rhyolitic composition: water (wt.%) = (43.51 ± 1.02) × $\Delta R/R_{\text{baseline}}$ − 0.004 (r^2 = 0.998).

desired samples, and partly because the Kramers-Kronig transform would introduce additional uncertainty as it requires a reflectance spectrum over spectral range much broader than the target peaks (Lichvár et al. 2002). Because the efficiency of the narrow-band MCT becomes very low beyond 800 to 5,500 cm^{-1}, obtaining data over a wavenumber range sufficiently wide for the Kramers-Kronig transform was not practical.

Because the noise of a spectrum is a major source of error in estimating water content, the degree of uncertainty depends on both aperture size and the number of scans. For example, with a 20 μm × 20 μm aperture and 2,048 scans, the uncertainty in ΔR (2σ) is 0.017. The uncertainty in ΔR can be approximately converted into uncertainty in water content by dividing ΔR by R_{baseline} and simultaneously multiplying by the slope of the regression line. Let, for example, R_{baseline} = 6 and let the slope = 49.76 (for basaltic composition), 0.14 wt.% uncertainty in water content is given. Table 2 summarizes the level of noise under various measurement conditions.

Table 2 Noise level in ΔR at different measurement conditions

Aperture size (μm)	Scan number	Noise level in R% (2σ)
100 × 100	512	0.0130
20 × 20	1,024	0.0250
30 × 30	1,024	0.0160
50 × 50	1,024	0.0105
100 × 100	1,024	0.0086
20 × 20	2,048	0.0170
30 × 30	2,048	0.0110

Application to natural samples

Natural glass samples (melt inclusions) have reflectance spectra similar to the synthetic glasses, which encouraged the application of the reflectance FT-IR method to natural samples. Figure 5 shows three spectra as examples, that is, basaltic melt inclusion hosted by olivine, basaltic melt inclusion hosted by plagioclase, and rhyolitic melt inclusion hosted by orthopyroxene. By applying their $\Delta R/R$ to the regression lines described above, their water contents were calculated to be 3.5, 3.1, and 2.8 wt.%, respectively.

Although the reflectance FT-IR method seems practical, two problems specific to analyzing natural samples were encountered. One involved an interference fringe pattern, which was sometimes observed in a reflectance

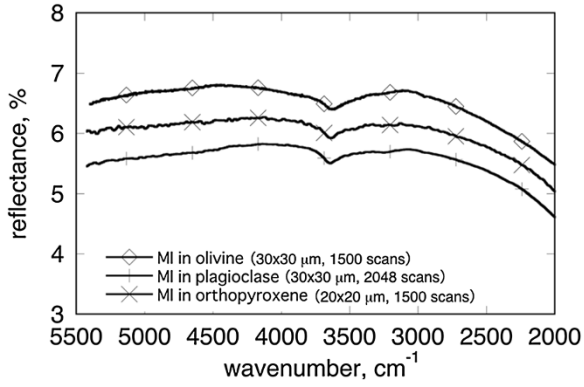

Figure 5 Examples of reflectance spectra measured from different melt inclusions. Natural melt inclusions (MI), olivine-hosted basaltic melt inclusion (diamond), plagioclase-hosted basaltic melt inclusion (+), orthopyroxene-hosted rhyolitic melt inclusion (×). The plots are offset for clarity.

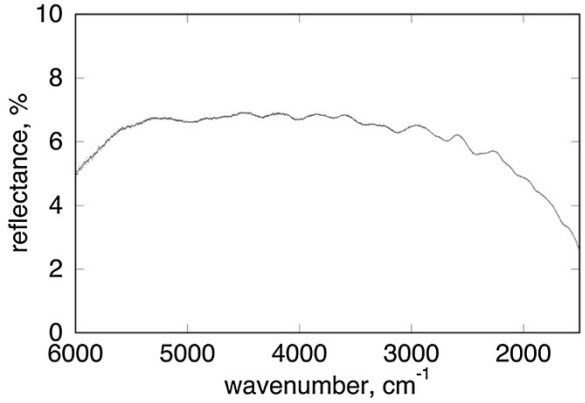

Figure 6 An example of interference fringe pattern. This was observed in a reflectance spectrum of plagioclase-hosted melt inclusion measured with an aperture of 20 × 20 μm and 2,048 scans.

spectrum. When a thin melt inclusion having a flat lower boundary to the host mineral is analyzed, reflection from the lower boundary overlaps with the light reflected from the surface. This resulted in the formation of an obstructive interference fringe pattern on the reflectance spectra (Figure 6). Interference fringes sometimes, but not always, occurred when a target sample was thin. This is because their occurrence is subject to many factors such as differences in refractive indexes between glass and host crystal, the shape of the boundary interface, aperture size of the reflection analysis, incident angle of infrared light, and so on. The number of waves found in the interval of wavenumbers between 2,000 and 3,000 cm^{-1} were usually less than five when interference fringes were observed. Consequently, the thickness of the melt inclusion was considered to be less than 17 μm, assuming that the refractive index of glass is 1.5. Anyway, we have not developed a good method to manage interference fringes on a reflectance spectrum yet. Therefore, we discarded the spectrum when interference fringes were observed on it. To expand the utility of the method, a project to manage the interference fringe pattern will be conducted in the future.

Another problem we sometimes encountered involved interference of host mineral. When analyzing small natural samples such as melt inclusions, some signals from the host mineral occasionally overlap the spectrum of the target sample, even though the aperture size is limited or very small. Therefore, applying the reflection FT-IR technique to small natural samples such as melt inclusions requires developing a method to correct for spectral overlap of the signal from host minerals.

Fortunately, the contribution of the host mineral to the spectrum of melt inclusion is easily recognized at 800 to 1,300 cm^{-1} because most minerals and glasses have unique reflectance spectra in this range (Duke and Stephens 1964; Pieters et al. 2008; Yasuda 2011). Figure 7, for example, compares the reflectance spectrum of a rhyolitic melt inclusion with that of its host orthopyroxene.

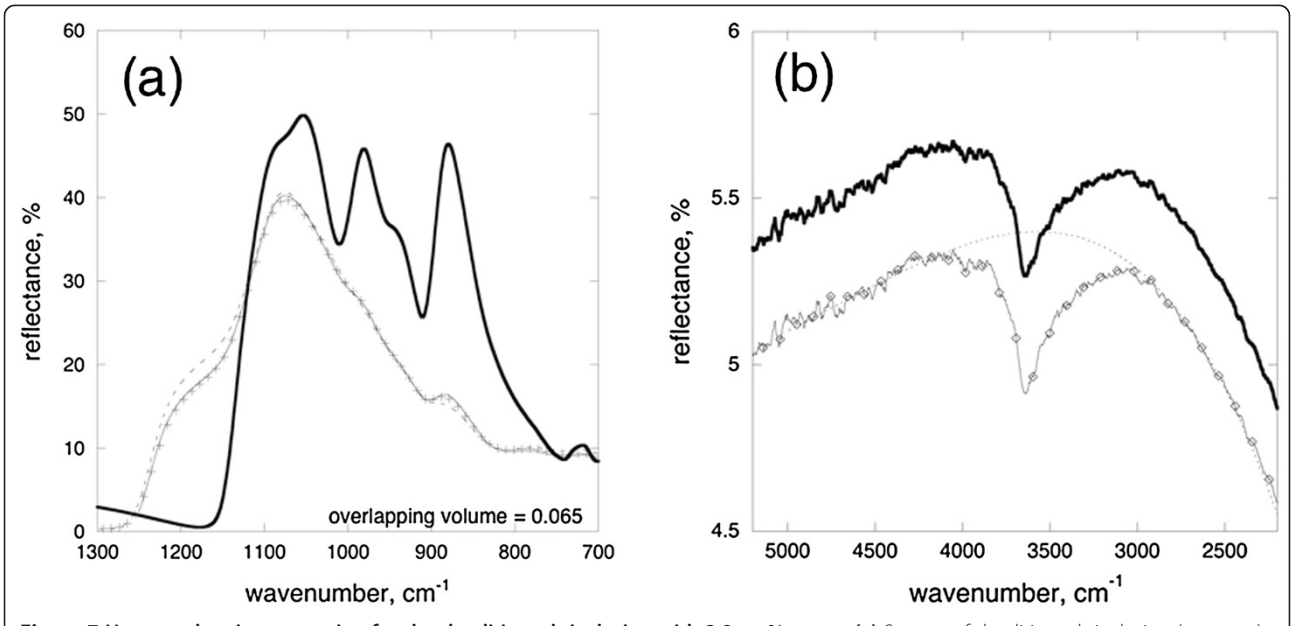

Figure 7 Host overlapping correction for the rhyolitic melt inclusion with 3.9 wt.% water. (a) Spectra of rhyolitic melt inclusion (m_x, cross), its host orthopyroxene (h_x, thick solid curve), and rhyolite glass (g_x, broken curve) in the 700 to 1,300 cm^{-1} region. The extent of the host mineral's overlap on the spectrum of melt inclusion was calculated to be 0.065 by curve fitting, and the calculated spectrum (f_x) is shown with a thin solid curve. **(b)** Using the overlapping volume obtained in (a), the original infrared (IR) spectrum of the melt inclusion (m_x, thick solid curve) in the 2,000 to 5,500 cm^{-1} region was modified (g_x, thin solid curve with open diamond), and the baseline curve (dotted curve) was calculated to obtain $\Delta R/R_{baseline}$.

The reflectance peak of rhyolitic glass was at 1,075 cm^{-1}, whereas the three reflectance peaks of orthopyroxene were at 1,055, 980, and 880 cm^{-1}. One of the peaks of orthopyroxene slightly overlapped the peak from the glass, but the other two peaks were clearly resolvable. Therefore, by using the relative intensities of the resolvable peaks, we can calculate the ratio of host crystals within the aperture, and thus the overlapping reflectance spectrum of the target melt inclusion (hereafter referred to as the overlapping volume).

Suppose both the melt inclusion and host crystal are observed in an aperture of, for example, 20 μm × 20 μm. If the reflectance from the pure melt inclusion at the wavenumber x is g_x, and if the reflectance from the host crystal is h_x, the calculated reflectance spectrum f_x from the entire aperture is $f_x = yh_x + (1 - y)g_x$, where y is the overlapping volume. When the actual measured spectrum is m_x, the overlapping volume y can be obtained when $S^2 = \Sigma(m_x - f_x)^2$ is a minimum (800 $cm^{-1} < x <$ 1,300 cm^{-1}). An example of curve fitting and the resultant overlapping volume are also shown in Figure 7a. The spectrum h_x is obtained by measuring the host crystal. In this case, it is very important to measure the host crystal at a point very close to the melt inclusion, because the peak position and the intensity of the reflectance spectrum are affected by crystal orientation and chemical composition. The glass spectrum g_x can be obtained by two ways. One way is to measure synthesized glass of similar composition. The other way, which is considered to be more practical, is to measure the same melt inclusion through a smaller aperture. Reflectance of silicate glass at 800 to 1,300 cm^{-1} is much stronger than the one at approximately 3,650 cm^{-1}. Therefore, a reduction of aperture size has little effect on the uncertainty caused by the noise. Once the overlapping volume, y, is obtained, the overlap-corrected spectrum g_x of melt inclusion at 2,000 to 5,500 cm^{-1} is calculated as $g_x = (m_x - yh_x)/(1 - y)$. By using the spectrum g_x, the $\Delta R/R_{\text{baseline}}$ ratio can be determined as described in the 'Methods' section. Figure 7b shows the corrected spectrum g_x together with the original melt inclusion spectrum m_x.

To what extent such overlap-correction is applicable is an important issue to address for this method. The overlap-correction method introduces additional uncertainties in determining water content because it requires measuring the host crystal and glass at 800 to 1,300 cm^{-1}. As the overlapping volume fraction approaches to unity, the uncertainty in $\Delta R/R_{\text{baseline}}$ becomes significantly larger than before because it approximately correlates with 1/(1 – (overlapping volume)). We made a series of measurements of a single large melt inclusion with known water content (3.1 wt.%) while changing the overlapping volume by shifting the aperture position. The results are summarized in Figure 8 and indicate that the water

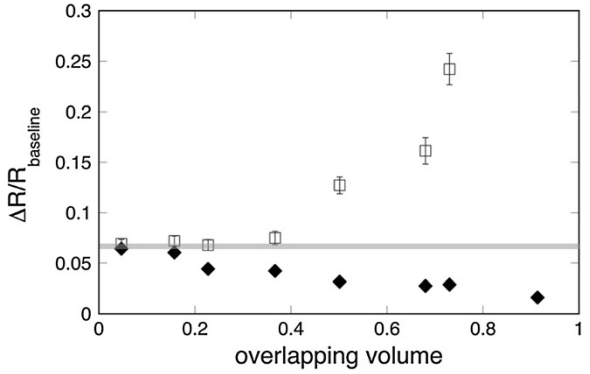

Figure 8 Effective range of overlap correction method tested by olivine-hosted melt inclusion. This was analyzed with an aperture of 20 × 20 μm and 1,024 scans. Open squares and solid diamonds are with and without the overlapping correction, respectively. Shaded line indicates $\Delta R/R_{\text{baseline}}$ (=0.062) when the overlapping volume, y, is zero. The water content of the sample was 3.1 wt.% when the regression equation for basaltic composition (slope = 49.76) was applied. If the uncertainty in y is negligible, the uncertainty in ΔR of the overlap-corrected spectrum approximately becomes $1/(1 - y)$ times larger. The error values thus estimated were added to the overlapping-corrected data. In actuality, the uncertainty in 'overlapping volume' may not be negligible; therefore, the error value presented here is considered to be a minimum value.

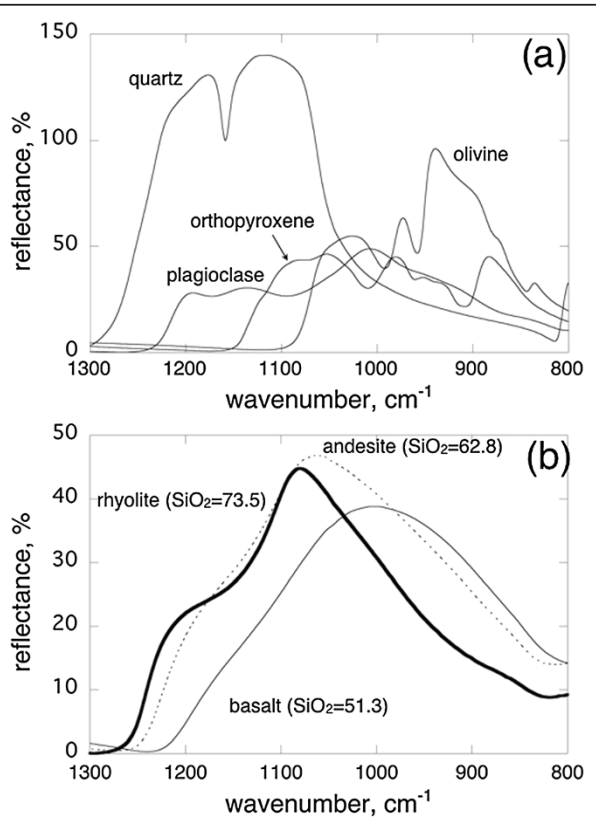

Figure 9 Infrared reflectance spectra of (a) some minerals and (b) silicate glasses.

content of the melt inclusion was correctly determined by the overlap correction method when the overlapping volume was less than 0.3. However, the discrepancy between the calculated value and the true water content became larger when the overlapping volume exceeded 0.4.

The correction method presented here seems effective at least for melt inclusions hosted by olivine, orthopyroxene, and plagioclase. Peaks in reflectance spectra obtained from several minerals are shown in Figure 9. Those of silicate glasses are also shown for comparison. Some peaks from the crystals mentioned above are quite different from those of silicate glasses. Therefore, the overlapping volume can be precisely calculated if a small amount of the host crystal is within the aperture used for measuring the melt inclusion. However, with this method, it may be difficult to determine the overlapping volume of quartz with reasonable precision. This is because two reflectance peaks from quartz are almost at the same position as those of silicate melt with high SiO_2 content, which is in chemical equilibrium with the host quartz.

Conclusions

By introducing a rotary pump and a narrow-band MCT detector into a FT-IR apparatus, we obtained a much better S/N ratio for reflectance spectroscopy. As a result, the water content could be quantified with reasonable accuracy (<0.3 wt.%) for melt inclusions with diameters as small as 20 μm and with a typical measuring time of 22 min.

We determined empirical relationships between the water content of silicate glasses and the variation in the reflectance intensity by linear least-square fitting of the analytical data: water (wt.%) = $49.76 \times \Delta R/R_{\mathrm{baseline}} - 0.08$ for basaltic composition, water (wt.%) = $46.74 \times \Delta R/R_{\mathrm{baseline}} + 0.10$ for andesitic composition, and water (wt.%) = $43.51 \times \Delta R/R_{\mathrm{baseline}} - 0.004$ for rhyolitic composition.

We developed a method to correct overlap of the melt inclusion spectrum with the spectrum from the host mineral. The method calculates the overlapping volume of the host crystal by fitting the reflectance spectra at 800 to 1,300 cm^{-1}, and then corrects the reflectance spectra at 2,000 to 5,500 cm^{-1} before calculating the water content. The method is applicable to melt inclusions hosted by olivine, orthopyroxene, and plagioclase. However, in order to be widely accepted as a reliable correction method for host-crystal overlapping, the method must be tested using a variety of melt inclusions - across different water contents, host mineral types, inclusion sizes, and shapes.

With this efficient analytical method, many melt inclusions including those with diameters as small as 20 μm can now be measured rapidly. This technique will contribute to improving our understanding of pre-eruptive volatile contents.

Competing interests
The author declares the he has no competing interests.

Acknowledgements
The author thanks Mika Goto, Miki Kurihara, Natsuko Takagi, and Natsumi Hokanishi for their help in performing FT-IR and Karl Fischer analyses. The author also thanks Toshitsugu Fujii for his valuable advice on the reflectance FT-IR method. The manuscript has been greatly improved by constructive comments from Dr. Geshi and two reviewers. This study was supported by JSPS KAKENHI Grant Numbers 23654182 and 22340159.

Received: 22 October 2013 Accepted: 30 April 2014
Published: 15 May 2014

References

Bureau H, Métrich N, Pineau F, Semet MP (1998) Magma-conduit interaction at Piton de la Fournaise volcano (Reunion Island): a melt and fluid inclusion study. J Volcanol Geotherm Res 84:39–60

Dixon JE, Stolper EM, Holloway JR (1995) An experimental study of water and carbon dioxide solubilities in mid-ocean ridge basaltic liquids: part I: calibration and solubility models. J Petrol 36:1607–1631

Duke DA, Stephens JD (1964) Infrared investigations of the olivine group minerals. Am Mineral 49:1388–1406

Grzechnik A, Zimmermann HD, Hervig RL, King PL, McMillan PF (1996) FTIR micro-reflectance measurements of the CO32- ion content in basanite and leucitite glasses. Contrib Mineral Petrol 125:311–318

Hervig RL, Mazdab FK, Moore G, McMillan PF (2003) Analyzing hydrogen (H_2O) in silicate glass by secondary ion mass spectrometry and reflectance Fourier transform infrared spectroscopy. In: De Vivo B, Bodnar RJ (ed) Melt inclusions in volcanic systems: methods, applications and problems. Elsevier, Amsterdam, pp 83–103

King PL, Larsen JF (2013) A micro-reflectance IR spectroscopy method for analyzing volatile species in basaltic, andesitic, phonolitic, and rhyolitic glasses. Am Mineral 98:1162–1171

Larsen JF (2008) Heterogeneous bubble nucleation and disequilibrium H_2O exsolution in Vesuvius K-phonolite melts. J Volcanol Geotherm Res 175:278–288

Lichvár P, Liška M, Galusek D (2002) What is the true Kramers-Kronig transform? Jour Ceramics-Silikáty 46:25–27

Lowenstern JB, Pitcher BW (2013) Analysis of H_2O in silicate glass using attenuated total reflectance (ATR) micro-FTIR spectroscopy. Am Mineral 98:1660–1668

Luhr JF (2001) Glass inclusions and melt volatile contents at Paricutin Volcano, Mexico. Contrib Mineral Petrol 142:261–283

Métrich N, Bertagnini A, Landy P, Rosi M (2001) Crystallization driven by decompression and water loss at Stromboli Volcano (Aeolin Islands, Italy). J Petrol 42:1474–1490

Métrich N, Wallace P (2008) Volatile abundances in basaltic magmas and their degassing paths tracked by melt inclusions. In: Putirka K, Tepley F (ed) Minerals, inclusions and volcanic processes. Reviews in Mineralogy and Geochemistry, vol 69. Mineralogical Society of America, Chantilly, Virginia, pp 363–402

Miller JN (1991) Basic statistical methods for analytical chemistry, part 2: calibration and regression methods, a review. Analyst 116:3–14

Moore G, Chizmeshya A, McMillan PF (2000) Calibration of a reflectance FTIR method for determination of dissolved CO_2 concentration in rhyolitic glasses. Geochim Cosmochim Acta 64:3571–3579

Pieters CM, Klima RL, Hiroi T, Dyar MD, Lane MD, Treiman AH, Noble SK, Sunshine JM, Bishop JL (2008) Martian dunite NWA 2737: integrated spectroscopic analyses of brown olivine. J Geophys Res 113:E06004. doi:10.1029/2007JE002939

Roggensack K, Hervig RL, Mcknight SB, Williams SN (1997) Explosive basaltic volcanism from Cerro Negro volcano: influence of volatiles on eruptive style. Science 277:1639–1642

Saito G, Kazahaya K, Shinohara H, Stimac J, Kawanabe Y (2001) Variation of volatile concentration in a magma system of Satsuma-Iwojima volcano deduced from melt inclusion analyses. J Volcanol Geotherm Res 108:11–31

Stolper EM (1982) Water in silicate glasses: an infrared spectroscopic study. Contrib Mineral Petrol 81:1–17

Suzuki Y, Yasuda A, Hokanishi N, Kaneko T, Nakada S, Fujii T (2013) Syneruptive deep magma transfer and shallow magma remobilization during the 2011

eruption of Shinmoe-dake, Japan—constraints from melt inclusions and phase equilibria experiments. J Volcanol Geotherm Res 257:184–204

Wallace PJ (2005) Volatiles in subduction zone magmas: concentrations and fluxes based on melt inclusion and volcanic gas data. J Volcanol Geotherm Res 140:217–240

Yasuda A (2011) FT-IR micro reflectance measurement of water content in melt inclusions. Bull Volcanol Soc Japan 56:41–49 (in Japanese with English abstract)

Zhang Y (1999) H_2O in rhyolitic glasses and melts: measurement, speciation, solubility, and diffusion. Rev Geophys 37:493–516

doi:10.1186/1880-5981-66-34
Cite this article as: Yasuda: **A new technique using FT-IR micro-reflectance spectroscopy for measurement of water concentrations in melt inclusions.** *Earth, Planets and Space* 2014 **66**:34.